RSC Advances

RSC Advances

Volume 1 | Number 1 | Jan 2013 | Pages 1–100

www.rsc.org/advances

ROYAL SOCIETY OF CHEMISTRY

Newly Reduced Graphene Oxide/Gold Oxide Neural-Chemical Interface on Multi-channels Neural Probe to Enhance Electrochemical Properties for Biosensors

Ta-Chung Liu[1], Chao-Yi Chu[1], You-Yin Chen[2] and San-Yuan Chen[1,*]

[1]Department of Materials Science and Engineering, National Chiao Tung University, No. 1001, Ta-Hsueh Rd., Hsinchu, Taiwan 300, R.O.C.

[2]Department of Biomedical Engineering, National Yang Ming University, No.155, Sec. 2, Linong St., Taipei, Taiwan 112, R.O.C.

[*]Correspondence should be addressed to either of the following:

Prof. San-Yuan Chen

Department of Materials Science and Engineering, National Chiao Tung University, No. 1001, Ta-Hsueh Rd., Hsinchu, Taiwan 300, R.O.C.

Email: sanyuanchen@mail.nctu.edu.tw;

Table of content

The newly neural-chemical interface designed by rGO-wrapped gold oxide nanocomposite on multi-channel neural probe as biosensor.

Abstract

In this study, a facile one-step Cyclic Voltammetry (CV) electrophoresis was proposed for designing reduced graphene oxide/gold oxide (rGO/AuO$_x$) modified electrode by using chloride ions (Cl$^-$) with simultaneous occurrence of gold oxidation and GO reduction to induce the intimate attachment of negatively charged rGO sheets on the positively charged Au$^+$/Au^{3+} clusters by electrostatic interaction. The surface microstructure and the oxygen functional groups of rGO/AuO$_x$ can be tuned by controlling the dissolution rate of gold via the deposition scan rate. At a low deposition scan rate, the rGO/AuO$_x$ electrode with well-dispersive rGO sheets and large active sites can induce the rapid electron transfer to promote H$_2$O$_2$ detection. The amperometric response results displayed a relative fast response of less than 5s with a low detection limit of 0.63 μM (S/N=3). Also, the rGO/AuO$_x$ neural-chemical interface can be modified at multi-channels on neural probe and exhibited excellent sensing performances to H$_2$O$_2$. The results demonstrated that the rGO/AuO$_x$ modified electrode integrated with an neural probe using this one-step electrochemical deposition can provide faster response and higher sensitivity by optimizing and controlling the surface microstructure of rGO/AuO$_x$, which would serve a platform for medical application as biosensors for multi-sensing.

1. Introduction

Over the past decade the development of non-enzymatic sensor has gained wide attention because the performances of enzyme-based assays are easily affected by the environmental condition such as temperature, pH, humidity, and the presentence of enzyme-poisoning molecules and enzymatic sensors are easily dampened by inflammatory response during implantation[1-3]. The fabrication of non-enzymatic biosensors with inorganic metal oxides, polymers, carbon materials, nanoparticles, and their composites have introduced good selective and highly responsive so that non-enzymatic sensors have become primary for *in vivo* sensing. Recently, the application of nanomaterials has gained considerable attention to address non-enzymatic sensor challenges by increasing geometry areas and chemical activity to enhance sensitivity and selectivity. These challenges directed us toward developing a nanocomposite modified electrode with improved electrochemical/electrical performances and sensitivity, particularly for micro-scale electrochemical sensors because of several advantages for the detection of biochemical signals compared to macroscopic counterparts: (1) higher spatial resolution because of small geometric area (i.e. selectivity)[4] (2) small RC (R: resistance, C: capacitance) time constants due to the reduced double layer capacitance, providing higher temporal resolution and faster electron transfer[5,6].

The performance of an electrode depends on the materials used and the ability to chemically modify its surface, which can be further tuned by controlling the architecture of the electrode interface using nanomaterials. Among different nanomaterials, graphene-based have drawn more attention due to its unique properties and highly amenable to micro-fabrication. Moreover, graphene oxide-based (GO-based) materials are electrochemically active toward redox-active species and achieve intimate connectivity with molecules on their surface due to their excellent electrical conductivity, mechanical properties, chemical stability, and biocompatibility[7]. Moreover, owing to their solution-processability[8], GO-based materials can be readily "functionalized" to enhance catalytic properties[9-14] and reduce thermal noise in recording signals[15]. However, certain problems such as aggregation or restacking were encountered in assembling a GO-modified metal-based

sensor due to the very weak intersheet van der Waals attractions and non-comparable bonding between metal and GO sheets. Many methods such as Langmuir-Blodgett deposition[16,17] have been employed to synthesize single or monolayer GO to resolve restacking issues and enable the film thickness to be controlled whereas the disadvantages of weak physical bonding by intermolecular forces and the addition of toxic materials during the manufacturing process must still be overcome. Other methods for overcoming the problems associated with GO sheet restacking have involved the intercalation of nanoparticles such as polymer particles and even carbon nanotubes in between GO sheets[18,19]. For instance, graphene nanosheets and chitosan are frequently used together because the positively charged chitosan can interact with the negatively charged graphene nanosheets to prevent their aggregation[20]. However, these synthesis processes are highly complicated because of the complex chemical reactions involved.

To solve the existing challenges and problems concerning GO-based deposition on metal electrodes, we proposed a novel facile process combined Cyclic Voltammetry (CV) with repetitive cycles and chloride ion (Cl^-) induction as shown in **Scheme 1.** More importantly, the microstructure of the rGO/AuO_x electrode can be altered by tuning the deposition scan rate so that controllable electrode-interface morphology can be obtained, which would further modify its defect density and oxygen functional groups. Hydrogen peroxide (H_2O_2) is closely related to human metabolism and the accumulation of H_2O_2 can cause grievous injury to cells through base modifications and strand breakage in genomic DNA. Owing to the importance of H_2O_2, the sensitive and precise determination of H_2O_2 is mandatory and highly appreciable. By using this unique one-step electrophoresis in this work, we made a proof-to-concept on multi-sensing by evaluating the sensing performance of H_2O_2 with the rGO/AuO_x nanocomposite electrodeposited on multi-channel neural probe. The results have demonstrated that the rGO/AuO_x nanocomposite modified electrode with tunable microstructures exhibited excellent sensitivity for H_2O_2 detection, implying the potential application in biosensors.

2. Materials and Methods

2.1 Preparation of graphene oxides

The small-sized GO sheets providing large amount of active sites for micro-biosensor were prepared using the modified Hummers method[21] from flake graphite (No. 332461, Aldrich, USA). Briefly, 10 g of graphite and 7.5 g of $NaNO_3$ were placed in a flask. Then, 750 mL of H_2SO_4 was added with stirring in an ice-water bath, and 45 g of $KMnO_4$ was slowly added over approximately 1 h. Stirring was continued for 2 h in the ice-water bath and remained stirring for 5 days at room temperature to obtain homogeneous solution. The homogeneous solution was maintained with stirring over approximately 1 h, at 98 °C. The resultant mixture was further stirred for 2 h at 98 °C. Next, as the temperature was reduced to 60 °C, 30 mL of H_2O_2 (30 wt % aqueous solution) was added, and the mixture was continuously stirred for 2 h at room temperature. To remove the ions of the oxidant and other inorganic impurities, the resultant mixture was purified by repeating the following procedure cycle 15 times: centrifugation, removal of the supernatant liquid, addition of 2 L of a mixed aqueous solution of 3 wt % H_2SO_4/0.5 wt % H_2O_2 to the bottom solid, and dispersing the solid using vigorous stirring and bath ultrasonication for 30 min at a power of 140 W. Then, a similar procedure was repeated three times using 3 wt % HCl aqueous solution (2 L) and one time using H_2O (2 L). Air-dried process was used to remove to obtain the desired GO sheets. The as-synthesized graphene oxide solution was subsequently purified by dialysis until its pH value reached 6.5, then was subjected to ultra-sonication for 1 h.

2.2. Preparation of rGO/AuOx modified electrode

Electrochemical synthesis was performed by CV using an electrochemical instrument (CHI 614C, CH Instruments, Inc., Austin, USA) with a three-electrode configuration, in which Ag/AgCl served as the reference electrode (No.002243, ALS Co., Ltd, Tokyo, Japan), a platinum mesh served as the counter electrode (No.002222, ALS Co., Ltd, Tokyo, Japan) and a neural probe[22] served as the working electrode. The gold electrode was in turn polished using 0.3 μm and 0.05 μm alumina

powders. The GO solution was ultra-sonicated, and nitrogen was bubbled to degas the medium. A neutral aqueous GO suspension (0.5 mg mL^{-1}, pH = 6.5) was mixed with the sodium chloride (NaCl) solution (100 mM) as the electrophoresis medium, in which NaCl was used as the electrolyte and an etching agent for the gold electrode. The rGO/AuO$_x$ nanocomposite was prepared using a scan range of -1.4 V to +1.4 V, within which the gold surface was dissolved at 1.25 V and electro-reduction of GO occurred at -1.0 V[23]. Additionally, we prepared rGO/AuO$_x$ modified electrodes with different deposition scan rates from 10 mVs^{-1} to 250 mVs^{-1}for further investigation.

2.3. Characterization of rGO/AuO$_x$ nanocomposite

The surface morphology of the rGO/AuO$_x$ nanocomposite was examined using scanning electron microscopy (SEM, JSM S6700, JEOL Ltd., Akishima-shi, Japan). The surface carbon structure of the nanocomposite was characterized using a DeltaNu® Raman spectrometer (Advantage 200A, SciAps, Inc., Woburn, USA). In addition, X-ray photoelectron spectroscopy (XPS, VG Escalab 250 iXL ESCA, VG Scientific,UK) was used to determine the elecmental composition and chemical bonding of the rGO/AuO$_x$ nanocomposite.

2.4. Electrochemical Characterizations

The surface kinetics and surface reactions of rGO/AuO$_x$ electrodes were examined at various scan rates in PBS (10, 20, 40, 80, 160, and 320 mVs^{-1}). The electrochemical performance of the rGO/AuO$_x$ electrodes with different deposition scan rates (10 mVs^{-1}, 50 mVs^{-1}, and 250 mVs^{-1}) was tested using CV in a 0.2 mM hydroquinone (HQ)/ 0.1 M phosphate buffered saline (PBS) solution, in which a platinum plate was used as the counter electrode and Ag/AgCl was used as the reference electrode.

2.5. Amperometric experiments of H_2O_2

In-vitro amperometric experiments were carried out using a conventional three-electrode system in artificial cerebral spinal fluids (aCSF, 125 mM NaCl, 2.5 mM KCl, 2 mM $CaCl_2$, 1 mM $MgCl_2$, 25 mM $NaHCO_3$, 1.25 mM NaH_2PO_4, 20 mM glucose, 5% CO_2, pH= 7.4), in which a neural probe incorporated with rGO/AuO_x nanocomposite with 10 mVs^{-1} (Channel 1-3 as defined in **Figure 3**) and non-coated electrode were used as the working electrodes. The buffer was purged with high-purity nitrogen for at least 30 min prior to each amperometric experiment aiming to protect the solution from oxygen. The amperometric measurements were carried out under stirring with the addition of H_2O_2. The successive injections of H_2O_2 concentration were 10 μM, 20 μM, and 50 μM for Electrode Channel 1 to Channel 3. The calibration plot was performed by amperometric test with detection ranging from 10 μM to 300 μM.

3. Results and discussion

3.1. Electrochemical deposition of rGO/AuO_x nanocomposite

Figure 1 shows the formation steps and the corresponding CV plot of a rGO/AuO_x nanocomposite in the range from -1.4 V to 1.4 V at 10 mVs^{-1} with 10 electrodeposition cycles. During the first anodic potential scan, a large anodic peak appeared at +1.25V[24]. Step ⓐ represented the dissolution of the gold electrode by chloride ions (Cl$^-$) in a GO/NaCl bath to form a positively charged surface, called the Au^+/Au^{3+} surface. Step ⓑ illustrated the electrochemical deposition of GO sheets on Au^+/Au^{3+} rough surface by electrostatic forces, and then the oxygen dissociated in water would be anchored in Au^+/Au^{3+} surface to form a hybrid GO/AuO_x nanocomposite. Step ⓒ, a small cathodic hump appeared at +0.6V, indicating the hydration of Au surface and the analogous formation of $Au(H_2O)_m^+$ or $Au(H_2O)_m^{3+}$. This provides further evidence for the Au^+/Au^{3+} ions formation in the solution during the electrochemical deposition of AuO_x on Au electrode with modifying by GO. Step ⓓ presented the electro-reduction of GO, leading to the formation of a rougher rGO/AuO_x nanocomposite. As it is well known that GO sheets are mostly

decorated with epoxy and hydroxyl groups on the basal plane, while carbonyl and carboxyl groups are located at the edges. During the electrochemical deposition process, the GO sheets with negatively charged oxygen functionalities would be attracted towards the positively charged Au^+/Au^{3+} ions from the bath solution by electrostatic driving force, and thus got anchored at the Au^+/Au^{3+} surface. Meanwhile, the oxygen dissociated from the water should be captured immediately by the anchored Au^{3+} ions, resulting in the formation of rGO/AuO_x composite.

3.2 Morphology and structure characterization of rGO/AuO_x nanocomposite

Figure 2(a) shows the top-view surface microstructure of an rGO/AuO_x nanocomposite, indicating that a blanket of wrinkled rGO sheets covered on the surface of the AuO_x as presented in a magnified image of **Figure 2**(b). The cross-section views with its magnified image in **Figure 2**(c) and **e 2**(d) showed that the flexible rGO sheets were observed to be tightly attached to the etched gold substrate (AuO_x layer), revealing that the surface morphology of the rGO/AuO_x nanostructure might be controlled by the AuO_x layer. Such a nanostructure with a few layers of rGO sheets provided a large number of active surface sites and a rapid mass transport rate due to the short diffusion distance from rGO to AuO_x. To conclude, the unique rGO/AuO_x nanocomposite exhibited a high surface area, a short diffusion distance across rGO sheets to AuO_x layer and the ability to tailor the surface morphology for improving the restacking of GO sheets on the electrode. Furthermore, we examine detailed morphological information of rGO/AuO_x nanocomposites by AFM as shown **in Figure 3**, showing that lots of sharp and smaller size protrusions, produced by chloride ions, were observed in rGO/AuO_x nanocomposites deposited with 10 mVs^{-1}, while the rGO/Au_2O_3 nanocomposites with 250 mVs^{-1} produced flattened and large bulks morphology. Furthermore, the increasing percentage of surface area and roughness (R_a) in rGO/AuO_x nanocomposites with 10 mVs^{-1}, 50 mVs^{-1} and 250 mVs^{-1} were estimated as 11.00%, 6.85%, and 3.95% and 85.8, 71.6, and 53.4 nm, respectively. These quantitative results demonstrated that the increase in surface area for the rGO/AuO_x nanocomposites with lower deposition scan rates had

great influence on electrocatalytic activity of the rGO/AuO$_x$ nanocomposite. **Figure 4** (a)-(c) shows the Raman spectra of rGO/AuO$_x$ nanocomposites fabricated over 10, 50, and 250 mVs^{-1} deposition scan rates. All spectra exhibited two prominent peaks at 1350 cm^{-1} and 1583 cm^{-1}, corresponding to the well-documented D and G bands, respectively. The I$_D$/I$_G$ ratio can be used to determine the degree of bond disorder and chain information concerning carbon materials[25]. As compared to GO, rGO exhibited a larger I$_D$/I$_G$ ratio, which indicated the restoration of sp^2 carbon and a decrease in the average size of the sp^2 domains upon the reduction of GO. The I$_D$/I$_G$ ratio of the rGO/AuO$_x$ nanocomposite (I$_D$/I$_G$ = 1.245) fabricated over 10 mVs^{-1} was larger than that over 50 and 250 mVs^{-1}(I$_D$/I$_G$=1.01 and I$_D$/I$_G$ = 0.938, respectively), indicating that the amount of oxygen functional groups on the rGO/AuO$_x$ nanocomposite may be controlled by tuning the deposition scan rates and more carboxyl functional groups on the GO plane were partially electro-reduced at 10 mVs^{-1}. As a result, a high electrical conductivity was obtained for the rGO/AuO$_x$ nanocomposites formed over low deposition scan rates   XPS was further used to characterize the rGO/AuO$_x$ nanocomposite as illustrated in **Figure 4**(d)-(e). The high-resolution XPS of the C1s region in **Figure 4**(d) reveals that Au and O bonded with carbon in three different electronic states: carbon with a binding energy (BE) centered at 290.0 eV, carboxyl groups with a BE at 292.0 eV, and carbonates with a BE at 298.4 eV. The XPS spectrum of the O1s core level is presented in **Figure 4**(e) which indicates that both C and Au bonded with oxygen as evidenced by the two peaks of 537.4 eV (Au-O) and 541.6 (C–O). The high peak intensity of Au-O indicated that the oxygen functionalities on the rGO layer might have been obscured by the strong absorption of the AuO$_x$ layer. The XPS results further proved that the etched gold electrode has been transformed into gold oxide, whereas no chemical bonding (i.e., only electrostatic forces) existed between rGO and AuO$_x$.

3.3 Interface properties tuning by deposition scan rates

The electron transfer kinetics are dependent on not only the density of electronic states but also the surface microstructure especially for the carbon basal planes with the edge plane defects[26],

which would affect the electrochemical/electrical properties and sensitivity of rGO/AuO$_x$. The surface morphology could be tailored by the ion (Cl$^-$)-induced effect to control the dissolution rate of gold, which was also strongly dependent on the deposition scan rate associated with rGO sheets due to strong electrostatic forces between rGO and AuO$_x$. Therefore, at a low deposition scan rate, a longer dissolution time enabled a larger coverage and high roughness structure to be generated, which promoted higher attachment amounts of rGO sheets on the AuO$_x$ layer. In contrast, when the electrochemical deposition occurred at a higher deposition scan rate, it would lead to lower coverage of the rGO/AuO$_x$. The kinetics of the electrode interface reaction can be illustrated by the CV plot of the AuO$_x$ films obtained in 0.2 mM HQ at various scan rates as shown in **Figure 5(**a). Note that the anodic and cathodic peak currents increased with the scan rate but the peak voltage (V_p) remained at the same position (58 mV) even though the scan rate varied. The results were referred to the rapid interface electron-transferring kinetics because the electron transfer was fast enough to maintain the equilibrium between the reduced and oxidized forms of the redox couple. By the Nernst equation, **Figure 5**(b) presented a plot of the oxidative peak currents (I_p) as a function of the square root of the scan rate for both the anodic and cathodic peaks. The result demonstrated that both the reductive and oxidative peak currents exhibited linearity with the square root of the scan rate over the range of 10-320 mVs^{-1}, suggesting that the redox process on the modified rGO/AuO$_x$ electrodes was predominantly diffusion-controlled mass transfer reactions.

The electrochemical properties of an modified rGO/AuO$_x$ determined by the electron transfer rate were usually reflected in ΔEp, which was strongly related to the coverage of electrode materials, stacking manners vertically or laterally across the electrode surface, and diffusion distance within materials or across the interface between different materials at a heterogeneous surface. The results in **Figure 5**(c) demonstrated that the redox peak current of the rGO/AuO$_x$ nanocomposite obviously increased with lowering deposition scan rates. The rGO/AuO$_x$ nanocomposite deposited at a low deposition scan rate (10 mVs^{-1}) with 10 cycles exhibited a narrowed ΔEp (58 mV) and high sensitivity to HQ (a high peak current of ~80 μA), approximately 3 times and 8 times than the bare

gold, respectively. This was attributed to the shortened diffusion distance from rGO to the AuO_x

layer due to the tight connections between rGO and AuO_x.

To understand the thickness effect of the rGO/AuO_x nanocomposites, multiple-cycle deposition

with a scan rate of 10 mVs^{-1} was performed, as illustrated in **Figure 5**(d). The value of ΔEp

decreased with increasing cycle number below 25 cycles, indicating that enhanced electron transfer

kinetics occurred because the coverage of the rGO/AuO_x nanocomposite increased with cycle

number on the electrode. However, the increase in ΔEp with cycle number above 25 cycles was

ascribed to the increased thickness of rGO on the AuO_x layer, thus resulting in difficulties in

transferring the electroactive species to the electrode due to the extended distance from the

molecules to the electrode surface. The appearance of the minimum ΔEp value at 25 cycles (31 mV)

revealed that the electron transfer kinetics were strongly correlated with the coverage and thickness

of rGO on the AuO_x layer, which could be easily controlled by adjusting the appropriate

electrochemical parameters, a distinct advantage over previously developed methods.

3.4 Selectivity and anti-interference of rGO/AuO_x electrode

The selectivity and anti-interference capability of the rGO/AuO_x nanocomposite were shown

in **Figure 6**. The effect of common interfering electroactive substances, including dopamine (DA,

50 μM), uric acid (UA, 50 μM), Glucose (50 μM) and H_2O_2 (50 μM) in aCSF on Cyclic

Voltammetry was assessed and presented in **Figure 6**(a). The reductive peaks were observed around

-0.32V, -0.25V, -0.21V and -0.5V for UA, glucose, DA and H_2O_2 in aCSF, respectively. . Based on

the above interference study, -0.5V was reasonably chosen as the operation voltage to enhance

selectivity against the main endogenous brain interference species in an amperometric response

because the applied voltage of -0.5V in this study can distinguish the reduction from those of other

electroactive substances. In the anti-interference study shown as **Figure 6**(b), an obvious

amperometric response (approximately 0.2 nA) appeared when 20 μM H_2O_2 was injected at first at

an operation voltage of -0.5 V, and then glucose (20 μM) was injected in the mixture solution.

When 20 μM H_2O_2 was added for the second time, the current changed proportionally

(approximately 0.2 nA) even with the existence of the interferents. Later, although AA (20 μM), UA (20 μM) and DA (20 μM) injections as interferences produced noises, they did not cause observable amperometric changes. This demonstrated that the developed rGO/AuO_x electrode showed a superior selectivity to H_2O_2 by applying specific voltages at -0.5 V.

3.5 H_2O_2 sensing performance of rGO/AuO_x

Overall, the rGO/AuO_x nanocomposites developed in this study exhibited high charge transferring rate ensured by the exceptionally high conductivity of graphene and nanostructured conductive pathways of gold oxide (AuO_x). As a result, the reduction/oxidation of H_2O_2 can be achieved on the rGO/AuO_x nanocomposites by operating at a low voltage. In this study, the fabricated rGO/AuO_x modified electrode at a deposition scan rate of 10 mV^{-1} with 25 cycles was verified to operate as non-enzymatic biosensors. **Figure 7** showed the real-time amperometric $i–t$ detection of rGO/AuO_x modified electrodes in multichannel neural probe (Channel 1-3 as defined in **Figure 7**(a) fabricated at 10 mVs^{-1}, where the electrode potential was performed at -0.5 V with N_2 saturated in aCSF at pH 7.4). The rGO/AuO_x modified electrode (Channel 1-3) responded to amperometric currents at injections concentration of H_2O_2 ranging from 10μM to 50μM. All rGO/AuO_x modified electrode obviously showed a clear stepwise, indicating that rapid oxidation/reduction reaction occurred at a very short response time, exhibiting fast electron kinetics. The current underwent a transient increasing phase in each injection step of adding H_2O_2 and then reached a dynamic equilibrium: this equilibrium current of all three rGO/AuO_x modified electrodes (Channel 1-3) was observed to increase linearly with injected H_2O_2 concentrations as shown in **Figure 7**(b). For the rGO/AuO_x deposited with 10 mVs^{-1}, the detection limit was 0.63 μM (signal to noise =3) and a response time less than 5s to reach 100% signals. The calibration plot was further indicative of the sensitivity of the rGO/Au_2O_3 electrode at 1024.8 nA/μM·cm^2 ($r^2 = 0.997$). The H_2O_2 sensitivity in the rGO/AuO_x electrode was closely correlated with oxygen functional groups, surface roughness of the modified electrodes and the inter-attachment between rGO and AuO_x. To

further consider the reuse stability, the rGO/AuO$_x$ electrode was determined over a period of 14 days with analysis carried out every day shown in **Figure 8**. The rGO/AuO$_x$ electrode was performed 5 times a day and the electrode was stored in 0.01 M PBS at 4 °C after test every day. The rGO/AuO$_x$ electrode was found to retain 96.1% (N=5) of its initial activity after 14 days. Compared to other rGO/metallic oxide-based H$_2$O$_2$ sensors, our probe sensor with rGO/AuO$_x$ electrode displays a lower detection limit as listed in **Table 1**, which is probably relate to the fact that the rGO/AuO$_x$ nanocomposite deposited with 10 mVs^{-1} could effectively promote a two-electron coupled with two-proton redox reaction between the H$_2$O$_2$ and the electrode due to its extraordinary electron transfer. To sum up, the rGO/AuO$_x$ neural-chemical interface on implantable multi-channel neural probe designed with this one-step electrodeposition exhibited great tunable characteristics including electrochemical properties, low electrical impedance and high catalytic ability by varying deposition scan rates, which showed the great potential in enzymatic or non-enzymatic biosensors for in-vivo neuronal chemical "multi-sensing" in brain.

4. Conclusions

We have synthesized an rGO/AuO$_x$ nanocomposite using a facile one-step electrochemical method through an ion (Cl$^-$)-induced process to tune the electrode interface with close electrostatic interaction between the negatively charged GO sheets and positively charged Au$^+$/Au^{+3} substrate. The rGO/AuO$_X$ nanocomposite with low deposition scan rate provides the intact fast electron transportation from rGO to induce electron transferring on the electrode and higher H$_2$O$_2$ sensitivity. Most importantly, this study suggests that the tunable microstructure of rGO/AuO$_X$ nanocomposite could provide an easy way in modifying micro-biosensors and bioelectronics on multi-sensing with rapid response, high sensitivity, and well affinity.

RSC Advances Accepted Manuscript

References

1.   M. Martín, P. Salazar, R. Villalonga, S. Campuzano, J. M. Pingarrón and J. S. González-Mora, *J. Mater. Chem. B,* 2014, **2**, 739-746.

2.   P. Salazar, R.D. O'Neill, M. Martin, R. Roche and J.L. Gonzalez-Mora, *Sens. Actuators, B,* 2011, **152**, 137-143.

3.   Y. Tan, W. Deng, C. Chen, Q. Xie, L. Lei, Y. Li, Z. Fang, M. Ma, J. Chen and S. Yao, *Biosens. Bioelectron.*, 2010, **25**, 2644–2650.

4.   G. S. Wilson and R. Gifford, *Biosens. Bioelectron.*, 2005, **20**, 2388-2403.

5.   K. Balasubramanian, *Biosens. Bioelectronic.*, 2010, **26**, 1195-204.

6.   C. P. Andrieux and J. M. Savéant, *Chem. Rev.*, 1990, **90**, 723-738.

7.   D. Chen, L. H. Tang and J. H. Li, *Chem. Soc. Rev.*, 2010, **39**, 3157-3180.

8.   D. Li and R. B. Kaner, *Science.* 2008, **320**, 1170-1171

9.   D. Chen, H. Feng and J. Li, *Chem. Rev.*, 2012, **112**, 6027–6053.

10. X. Zhao, P. Zhang, Y. Chen, Z. Su and G. Wei, *Nanoscale*, 2015, **7**, 5080-5093

11. J. Ding, S. Zhu, T. Zhu, W. Sun, Q. Li, G. Wei and Z. Su, *RSC Adv.*, 2015, 5, 22935-22942

12. J. Ding, W. Sun, G. Wei and Z. Su, *RSC Adv.*, 2015, **5**, 35338-35345

13. P. Zhang, Y. Huang, X. Lu, S. Zhang, J. Li, G. Wei and Z. Su, *Langmuir*, 2014, **30**, 8980-8989.

14. P. Zhang, X. Zhang, S. Zhang, X. Lu, Q. Li, Z. Su and G. Wei, *J. Mater. Chem. B,* 2013, **1**, 6525-6531.

15. M. Pumera, A. Ambrosi, A. Bonanni, E. L. K. Chng and H. L. Poh, *TrAC, Trends Anal. Chem.*, 2010, **29**, 954-965.

16. Z. Qingbin, B. Zhang, X. Lin, X. Shen, N. Yousefi, Z. D. Huang, Z. Li and J. K. Kim. *J. Mater. Chem.*, 2012, **22**, 25072–25082.

17. X. Li, G. Zhang, X. Bai, X. Sun, X. Wang, E. Wang, E and H. Dai, *Nat. Nanotechnol.*, 2008, **3**, 538-542.

18. D. S. Su and R. Schlögl, ChemSuschem, 2010, **3**, 136-168.

19. H. C. Schniepp, J. L. Li, M. J. McAllister, H. Sai, M. Herrera-Alonso, D. H. Adamson, R. K. Prud'homme, R. Car, D. A. Saville and I. A. Aksay, *J. Phys. Chem. B*, 2006, **110**, 8535-8539.

20. H. Yin, Q. Zhang, Y. Zhou, Q. Ma, T. Liu, L. Zhu and S. Ai, Electrochim. Acta, 2011, **56**, 2748–2753.

21. N. I. Kovtyukhova, P. J. Ollivier, B. R. Martin, T. E. Mallouk, S. A. Chizhik, E. V. Buzaneva and A. D. Gorchinskiy, *Chem. Mater.*, 1999, **11**, 771-778.

22. Y. Y. Chen, H. Y. Lai, S. H. Lin, C. W. Cho, W. H. Chao, C. H. Liao, S. Tsang, Y. F. Cheng and S. Y. Ling, *J. Neurosci. Methods*, 2009, **182**, 6-16.

23. L. Chen, Y. Tang, K. Wang, C. Liu and S. Luo, *Electrochem. Commun.*, 2011, 13, 133–137.

24. R. P. Frankenthal and D. J. Siconolfi, *J. Eectrochem. Soc.*, 1982, **129**, 1192-1194.

25. A. C. Ferrari, J. Robertson, *Phys. Rev. B*, 2001, **64**, 075414.

26. N. Jia, Z.Wang, G. Yang, H. Shen and L. Z. Zhu, *Electrochem. Commun.* 2007, 9, 233-238.

27. F. Xu, M. Deng, G. Li, S. Chen and L. Wang, *Electrochim. Acta*, 2013, **88**, 59–65.

28. M. Liu, R. Liu and W. Chen, *Biosens. Bioelectron.*, 2013, **45**, 206–212.

29. S. Palanisamy, S. M. Chen and R. Sarawathi, *Sens. Actuators, B*, 2012, **166–167**, 372–377.
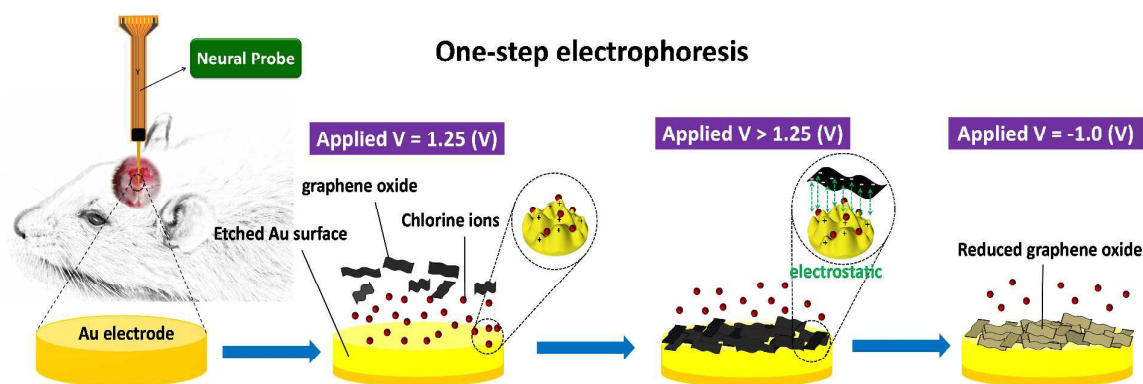
Schematic view. The experimental newly neural-chemical interface designed by reduced graphene oxide-wrapped gold oxide nanocomposite (rGO/AuO$_x$) via chloride ion (Cl$^-$)-induced effect on multi-channel neural probe.
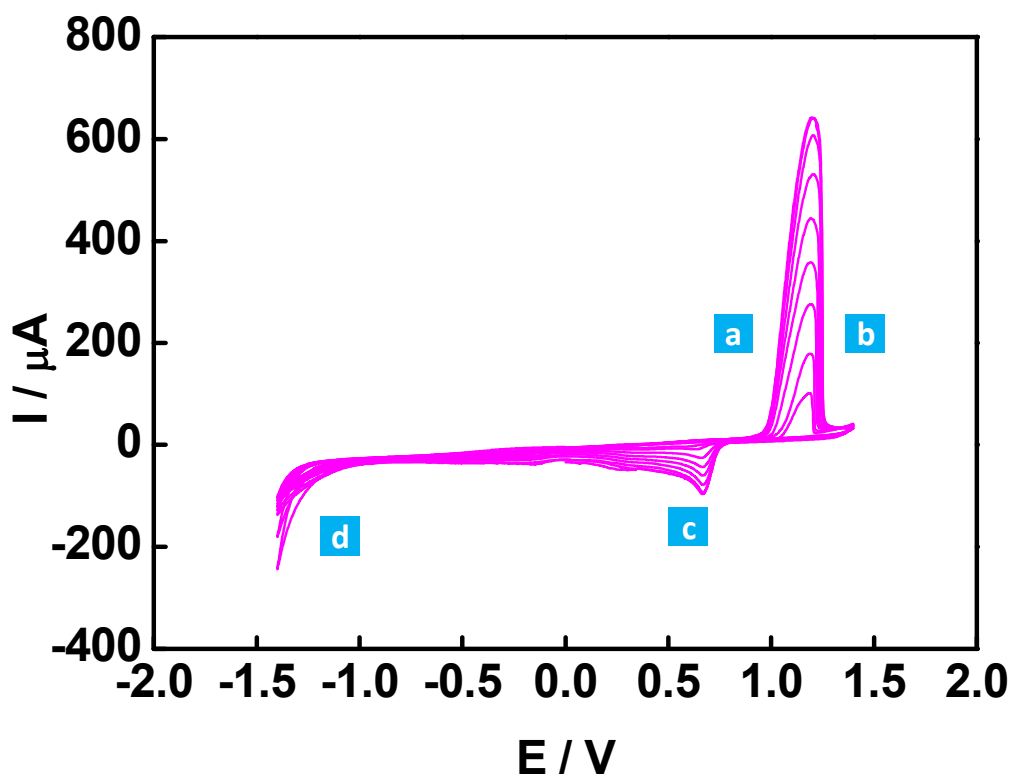

Figure 1. Real-time CV plot for the electrodeposition formation of the rGO/AuO$_x$ nanocomposite with 10 cycles was indicated with the letters corresponding to the manuscript.
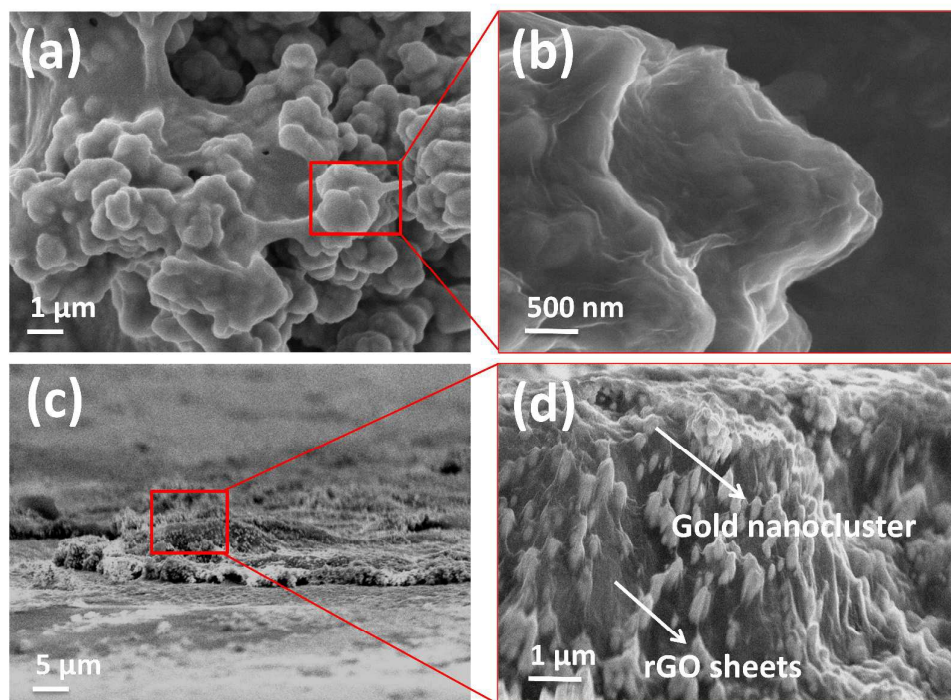
Figure 2. SEM images of the rGO/AuO$_x$ nanocomposite with 10 mVs^{-1}. (a)Top view and (b) its magnification view, (c) cross section view and (d) its magnification view. The rGO/AuO$_x$ nanocomposite showed that wrinkled rGO sheets were wrapped onto microporous gold oxide electrodes.
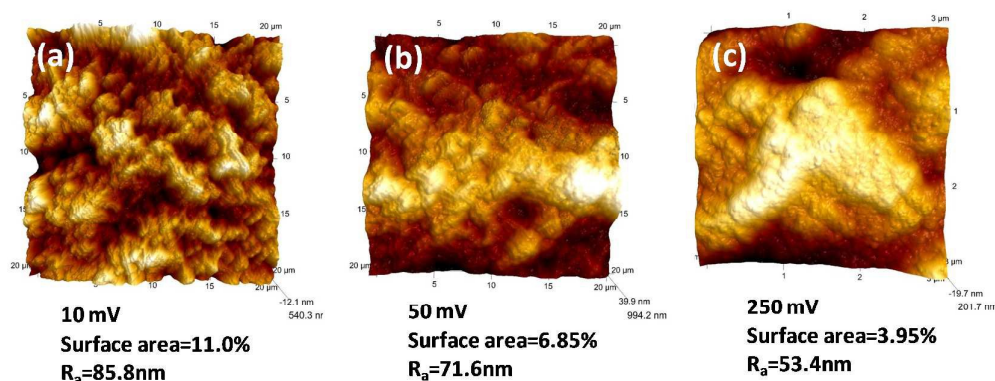

Figure 3. Topographical views of rGO/AuO$_x$ electrodes at 10 mVs^{-1}, 50 mVs^{-1}, and 250 mVs^{-1} obtained by atomic force microscopy (AFM) analysis. The corresponding increasing surface area percentages and roughness (R$_a$) were measured as 11.00%, 6.85%, and 3.95% and 85.8, 71.6, and 53.4 nm, respectively.
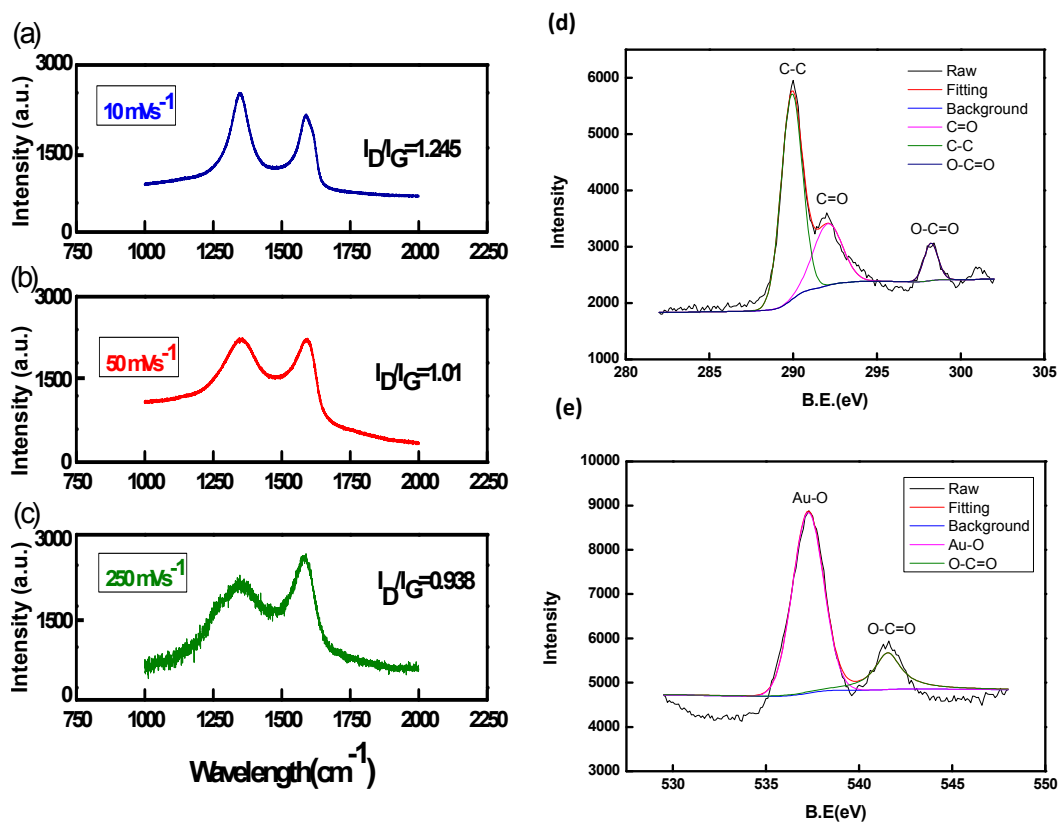
**Figure 4.** (a)-(c) Raman spectra of rGO/AuO$_x$ nanocomposite with different deposition scan rates. The G-band and the D-band were attributed to the first-order scattering of the E$_{2g}$ vibration mode in the graphite sheets and structural defects (disorder-induced modes), respectively. (d) XPS data of the C1$_s$ region of the rGO/AuO$_x$ film showing the carbon spin-orbit splitting of 1 s. (e) The O1$_s$ regions of the rGO/AuO$_x$ film showing the oxygen spin-orbit splitting of 1 s.
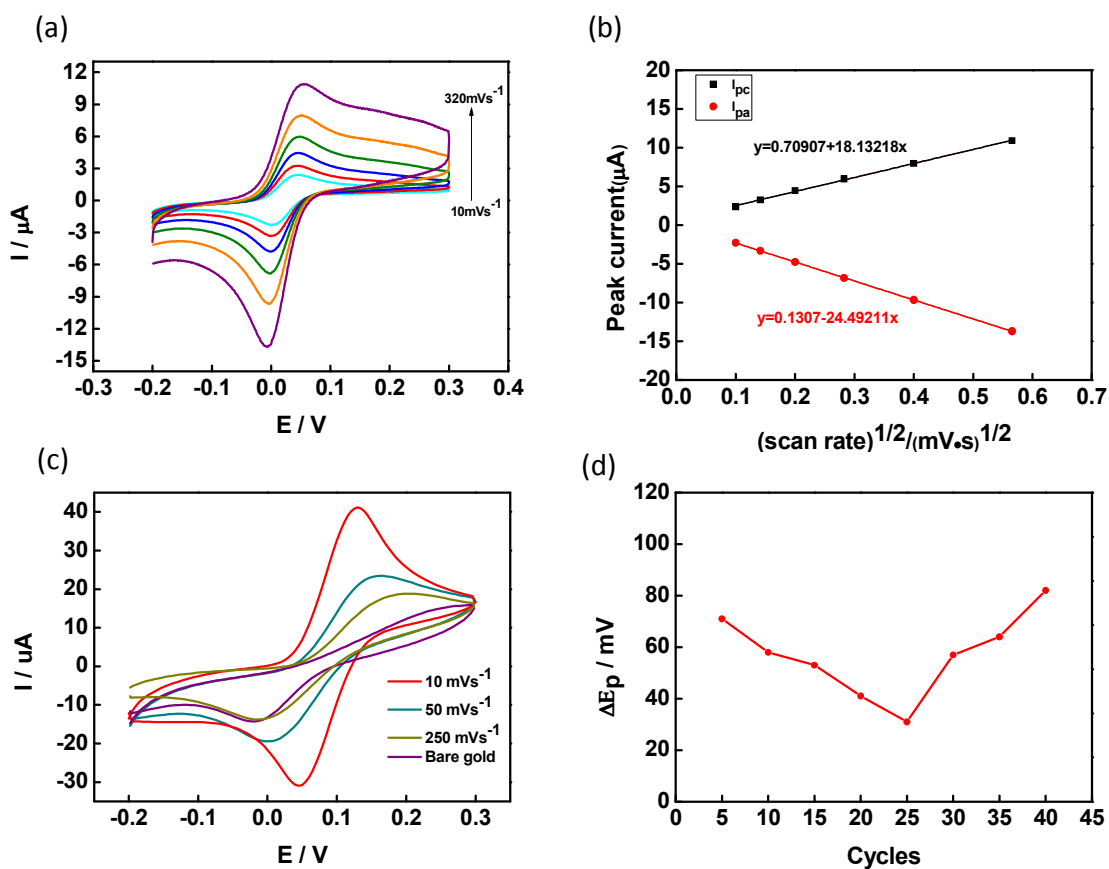
Figure 5. (a) CVs of 0.2 mM HQ in 0.1 M PBS rGO/AuO$_x$ at various scan rates (from inner to outer: 10, 20, 40, 80, 160, and 320 mVs^{-1}). (b) Linear calibration plot of rGO/AuO$_x$ nanocomposite：redox peak current vs. square root of the scan rate. (c) CVs of the rGO/Au$_2$O$_3$ electrode with different deposition scan rate of 10, 50, 250 mV^{-1} and non-coated gold electrode at 0.2 mM HQ in PBS. (d) Dependence plot of peak-to-peak potential separation (ΔEp) and peak-to-peak current ($\triangle$Ip) for various deposition cycles for rGO/AuO$_x$ film at 10mVs^{-1}.
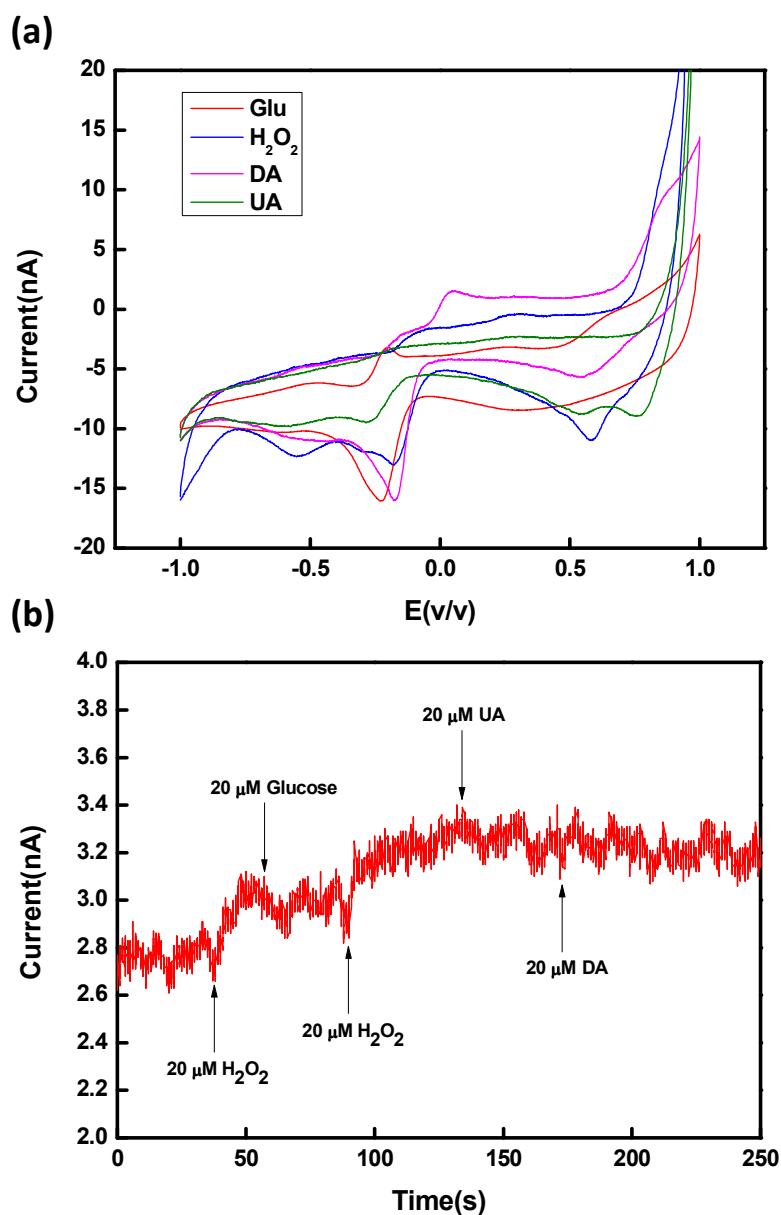
Figure 6. (a) CVs recorded with rGO/AuO$_x$ electrode at Glucose (50 μM), H$_2$O$_2$ (50 μM), DA (50 μM) and UA (50 μM) in artificial cerebrospinal fluid (aCSF) measured in the potential ranging from -1.0V to 1.0 V. (b) Current-time response curve at rGO/AuO$_x$ electrode for successive injection of Glucose (20 μM), H$_2$O$_2$ (20 μM), DA (20 μM) and UA (20 μM) in aCSF at -0.5 V.

RSC Advances Accepted Manuscript
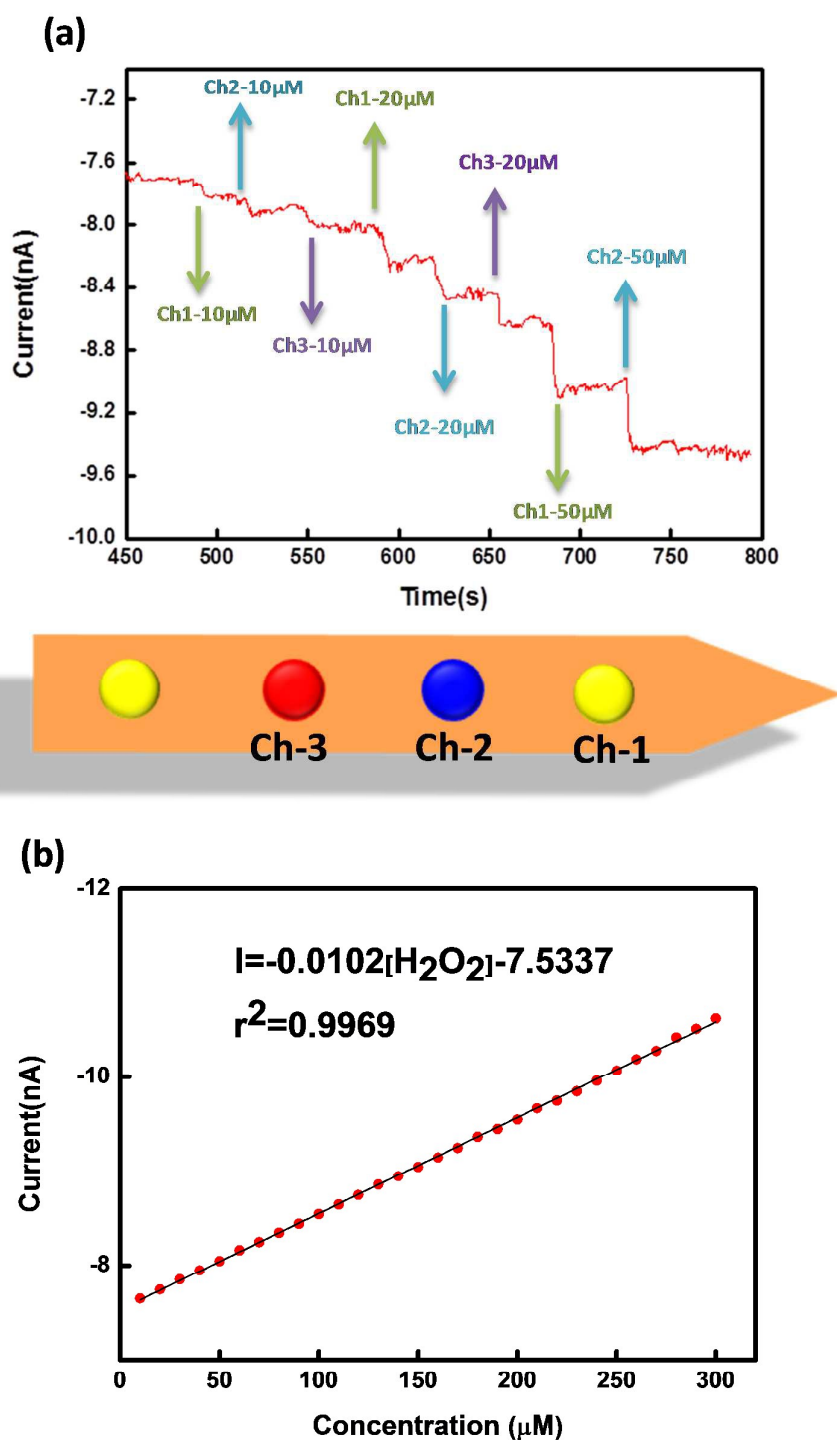
Figure 7. (a) The multi-channel amperometric response to H_2O_2 of rGO/AuO$_x$ modified electrodes at operation voltage of -0.5 V. (b) The calibration plot for rGO/AuO$_x$ modified electrode of Channel-1 showed the sensitivity of 1024.8 nA・$\mu M^{-1}/cm^2$ (The geometric area is 995.32 μm^2) with detection limit at 0.63 μM (S/N=3).

RSC Advances Accepted Manuscript
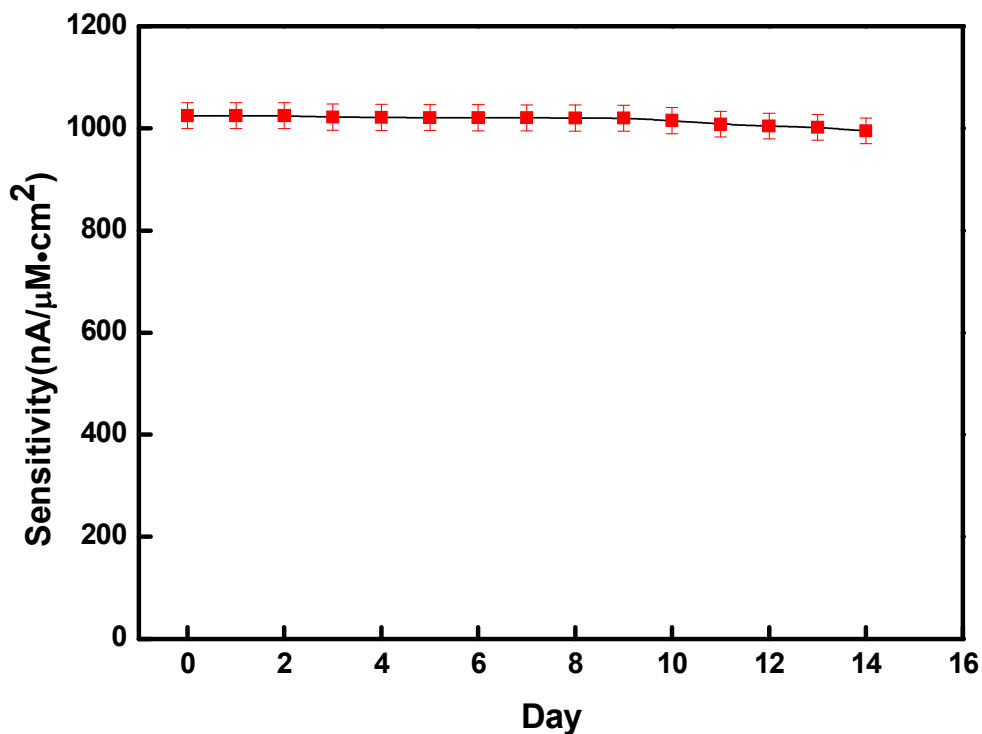
Figure 8. The reuse stability test of the rGO/AuO$_x$ electrode by measuring sensitivity over 14 days (N=5).

Table 1.   Comparison of several typical rGO/metallic-based H$_2$O$_2$ sensors.

Sensors	Applied potential (V)	Response time (s)	Detection limit (μM)	Reference
rGO/AuO$_x$	-0.5	<5	0.63	This work
rGO/AuNPs	-0.294	-	6.2	[14]
Cu$_2$O–rGO	-	-	21.7	[27]
Cu$_2$OMS–rGO	-0.24	-	10.8	[12]
Cu$_2$O nanocube–rGO	-0.4	<7	20.8	[28]
ZnO–rGO	-0.38	<5	0.02	[29]

AuNPs: gold nanoparticles; MWCNTs: multiwall carbon nanotubes; MS: microspheres